Photo-, Thermal-decomposition in Methylammonium Halide Lead Perovskites and inferred design principles to increase photovoltaic device stability

Emilio J. Juarez-Perez, Luis K. Ono, Maki Maeda, Yan Jiang, Zafer Hawash, Yabing Qi*

Energy Materials and Surface Sciences Unit (EMSSU), Okinawa Institute of Science and Technology Graduate University (OIST), 1919-1 Tancha, Onna-son, Okinawa 904-0495, Japan

*E-mail: Yabing.Qi@OIST.jp

Keywords

Perovskite Solar Cells; Stability; Photodecomposition; Encapsulation; Methylammonium Lead Iodide; Lead Iodide

Abstract

Hybrid lead halide perovskites have emerged as promising active materials for photovoltaic cells. Despite superb efficiencies achieved, it has been widely recognized that long-term stability is a key challenge intimately determining the future development of perovskite based photovoltaic technology. Here, we present reversible and irreversible photodecomposition reactions in methylammonium lead iodide ($MAPbI_3$). Simulated sunlight irradiation and temperature (40 ~ 80°C) corresponding to solar cell working conditions lead to three degradation pathways, (1) CH_3NH_2 + HI (identified as the reversible path), (2) NH_3 + CH_3I (irreversible or detrimental path), and (3) a reversible Pb(0) + I_2(g) photodecomposition reaction. If only reversible reactions (1) and (3) take place and reaction (2) can be avoided, encapsulated $MAPbI_3$ could be regenerated during the off-illumination timeframe. Therefore, to further improve operational stability in hybrid perovskite solar cells, photo-, thermal-degradation processes have to be mitigated with detailed understanding. First, the device encapsulation is necessary not only to avoid contact of perovskite with ambient air, but also to prevent leakage of volatile products released from perovskite. Second, a careful selection of organic cations in the perovskite compositional formula is needed to avoid any irreversible reaction. Third, selective contacts must be as chemically inert as possible against volatile released products. Finally, hybrid halide perovskite material is assumed to undergo a dynamic of formation and decomposition process and this could gradually decrease perovskite's crystalline grain size with time. Therefore, efforts on depositing highly and large crystalline perovskites could be efforts in vain in regards to the long-term stability.

Broader Context

In the past few years, perovskite solar cells have received tremendous attention and research efforts. The maximum attainable power conversion efficiency has been pursued with grand success. On the other hand, the research community of perovskite solar cells has recently realized that the device operational stability issue is currently the main obstacle impeding commercialization. At present, degradation processes in hybrid perovskite have been attributed mainly to external agents such as moisture and oxygen. In this work, we demonstrate that hybrid iodide perovskite suffers a photo-, thermal-decomposition reaction at mild conditions in a similar way as one of its parent lead iodide compound. Fortunately, this photodecomposition process can be almost reversed completely. To achieve long-term stability, perovskite material needs to be kept in a thermodynamic closed system where only reversible dynamic process of decomposing and self-healing take place establishing a chemical equilibrium between gas phase and solid components of the light harvester material.

Introduction

Hybrid lead halide perovskites have been intensively evaluated as light harvesting materials for photovoltaic cells since 2009.[1] Currently, long-term stability of perovskite solar cells is one of the major challenges where substantial efforts are needed to move forward hybrid perovskite solar cells towards commercialization.[2] Meanwhile, a significant number of research groups are achieving power conversion efficiencies over 20% using hybrid perovskite devices,[3] very few devices have succeeded in operational stability tests showing lifetimes longer than 1000 hours at the maximum power point.[3] Although promising attempts have been realized recently to improve durability of these cells by using different approaches as chemical inert scaffolds and electrodes,[4] or mixed/multication hybrid perovskites.[5] How hybrid perovskite suffers from degradation and what products are generated during the degradation are important questions to be answered in order to design stable perovskite-based solar cells. Furthermore, understanding of reversible degradation routes or the so-called self-healing in perovskite solar cells, which the cell performance recovers to the original value after resting in dark, has recently received attention as a strategy to prolong lifetime.[6] In the decomposition pathways of methylammonium based perovskites, the must-avoided degradation processes are irreversible degradation reactions limiting life time of the solar cells permanently. Therefore, the understanding of fundamental processes taking place in both reversible and irreversible degradation pathways is a step forward to advance in enhancing the stability of solar cells. Our group recently found that $MAPbI_3$ perovskite degrades significantly faster upon exposure to I_2 vapor than H_2O, O_2, or light only.[7] As highlighted by Wilks and Bär,[8] we proposed that the internally generated I_2 and its migration within $MAPbI_3$ induced by solar cell operation and/or external stimuli (such as H_2O, O_2, light irradiation, applied bias, and heat) leads to a self-sustaining and irreversible degradation reaction in perovskites independent of device architecture.[7] Additionally, we recently showed that CH_3I

and NH_3 are generated as irreversible gas by-products during high temperature thermal degradation of $MAPbI_3$.[9] However, the condition in which detrimental I_2 is generated remains unclear.

Interestingly, this missing puzzle is associated to a work published by Dawood *et al.* in half a century ago regarding lead iodide (PbI_2).[10] PbI_2 is a relevant material in the topic of perovskite solar cells. For example, PbI_2 is a regular reagent choice to synthesize hybrid perovskite and also it is the unique remaining degradation solid product after degradation of $MAPbI_3$. Dawood *et al.* found that PbI_2 suffers photodecomposition to iodine gas (I_2) and lead (Pb^0) upon interaction with visible light by observing electrical conductivity drop under illumination wavelengths above PbI_2 band gap.[10] They, then, suggested the following stepwise PbI_2 photodecomposition route: (I) photodecomposition of PbI_2 takes place assisted by two excitons generation mechanism (two electron-hole pairs); (II) these two excitons react, leading to formation of a Pb^0 atom, and (III) formation and release of I_2 molecule leaving two positive charged anion vacancies sites ($V_I^{\cdot}$),[11] see Figure 1a.

By reexamining Dawood *et al.*'s work, here we present the following two points: (1) systematical investigation of light-only decomposition pathways of PbI_2 by checking that our experimental setup (Figure1b) is able to detect I_2 release and then to pursue gas release detection on $MAPbI_3$ and (2) photodecomposition experiments on $MAPbBr_3$ aiming to shed light on "*why $MAPbBr_3$ stability is higher than $MAPbI_3$ perovskite?*"

Our experiments were performed in a home-built small vacuum chamber in the absence of H_2O and O_2 eliminating all other possible external degradation factors. Inside this vacuum chamber, applied light and/or heat and measured temperatures were accomplished *in situ* directly on the sample holder, and the released gaseous species during photodecomposition were probed using

a quadrupole mass spectrometer (MS) equipped with an electron multiplier detector. Based on this setup, light induced activation energies for I_2 release from PbI_2 and $MAPbI_3$ were extracted and compared. Thin-films of PbI_2, $MAPbI_3$ and $MAPbBr_3$ materials before and after photodecomposition procedure were studied by X-ray photoelectron spectroscopy (XPS) and X-ray diffraction (XRD) to identify the remaining non-volatile degraded solid products. Finally, we also investigated whether photodegraded PbI_2 films containing Pb^0 could be recovered to PbI_2 by exposing to I_2 pellets at room temperature, which showed the reversibility of this photodecomposition. We propose that hybrid lead halide perovskite materials under mild visible illumination and temperature conditions is reversible; *i.e.*, a continuously decomposing and re-forming dynamical process takes place, which establishes a chemical equilibrium between gas phase components and solid perovskite.

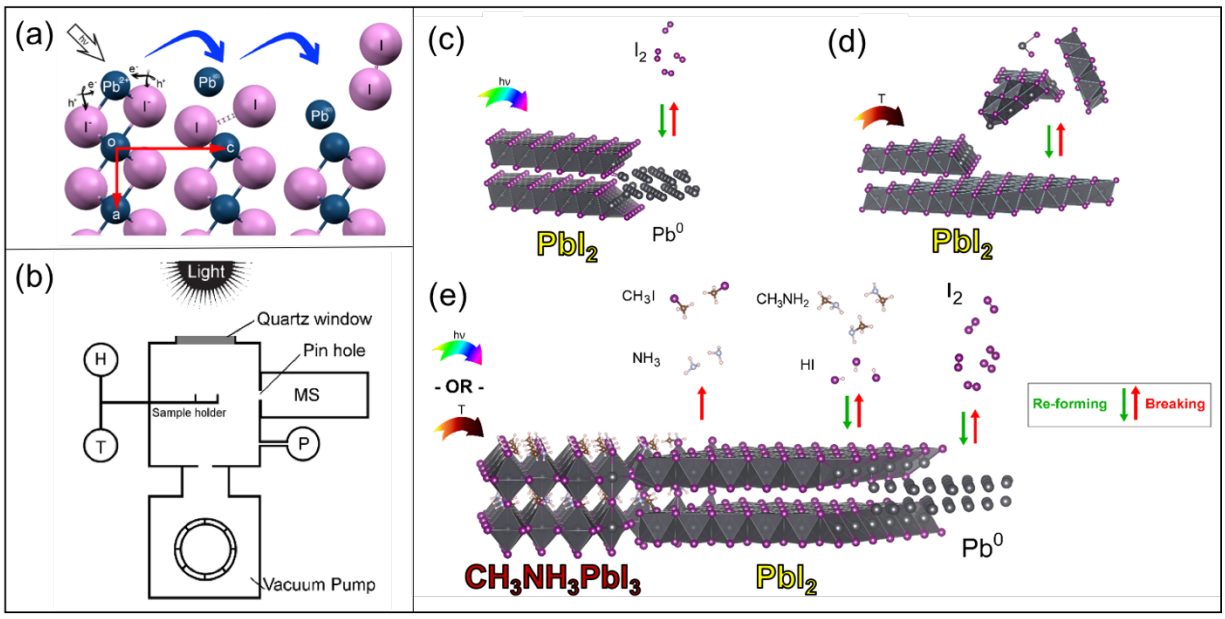

Figure 1 | Schematic illustration of photodecomposition, thermal evaporation and thermal degradation processes in PbI_2 and $MAPbI_3$. a) (0*k*0) plane view of layered PbI_2 supercell. The figure depicts the two steps for the release of I_2 and generation of Pb^0 by the two-exciton mechanism. b) Schematic drawing of the experimental setup for controlled PbI_2 and perovskite degradation experiments. H: electrical heater, T: thermocouple, P: crystal/cold cathode pressure gauge, MS: quadrupole mass spectrometer, top quartz window and Xe lamp or LED light sources with controlled on/off intervals. c) PbI_2 decomposition process driven by visible light (< 530 nm) above PbI_2 band gap at 40-60 °C, d) Temperature assisted PbI_2 evaporation at ~70 °C in dark, and e) $MAPbI_3$ photodecomposition and thermal degradation processes leading to irreversible decomposition to organic volatile gas species ($CH_3I + NH_3$), reversible decomposition ($CH_3NH_2 + HI$), and reversible generation of I_2 and non-volatile Pb^0 under illumination or mild heat conditions. Irreversibility of the process releasing $CH_3I + NH_3$ is indicated by one-directed arrow for the reaction. Crystal phases database used for depicting the structures were ICSD-68819 for PbI_2, ICSD-96501 for the cubic Fm-3m Pb^0 phase and ICSD-238610 for tetragonal $MAPbI_3$. Correlated partial occupation for methylammonium cation in $MAPbI_3$ phase was solved using Supercell.[12]

Results and discussion

PbI_2 degradation under illumination and dark conditions.

First, we performed the photodecomposition experiments on PbI_2 (Figure 1c) in our home-designed experimental setup (Figure 1b) to verify the adequacy of this setup for I_2 detection prior to compare with photodecomposition on $MAPbI_3$. Two important findings by Dawood *et al.*[10] were: (1) I_2 gas and metallic Pb^0 generations as a consequence of PbI_2 photodegradation with activation energy (E_a) of 4.7 kcal/mol, and (2) a threshold wavelength of 520 nm, where only higher photon energies initiate the photodecomposition of PbI_2. These findings were also observed in our set-up free moisture and anaerobic regimes but detecting I_2 gas release at temperatures as low as 40-60 °C. We probed four different pulsed light sources, three LED light sources: red (617 nm), blue (470 nm), white (450 + 550 nm) and Xe lamp based simulated solar irradiation (0.55 Sun). Also, an experiment at dark conditions but heating the sample stage at similar temperature level as during lightning experiments was carried out to decouple photodecomposition and thermal degradation (or evaporation) processes (Figure 1d). Details of experimental procedures are found in Methods section and Supplementary Information file. Next, experimental E_a for the I_2 release during PbI_2 photodecomposition process was extracted in order to determine the feasibility of this photodecomposition reaction. In our analysis, the corresponding I_2 release using different light sources were estimated from MS data trace pulses, see Table 1.

147 **Table 1**. Estimated* activation energies (E_a, kcal/mol) corresponding to I_2 release reaction (eq.
148 1).

Light Source	Wavelength (nm)	Temperature (°C)	Light Intensity (mW/cm^2)	E_a (kcal/mol)
White LED	450 + 550	50-70	80-110	57
Blue LED	470	45-62	71-120	45
Xe lamp	~ Sun	35-78	55	9

149 *Details on E_a determination and wavelength spectra distribution for each light source are shown
150 in Supplementary Sections S4 and S5, respectively.

151

152 E_a showed strong dependence in magnitude and wavelength distribution of light source
153 employed. The simulated sun light (Xe lamp, Table 1), which has a broader spectral wavelength
154 lead to the smallest E_a ~ 9 kcal/mol compared to narrow wavelength interval generated by LEDs
155 (E_a ~ 45 k/cal and 57 kcal/mol for blue and white LEDs, respectively). Interestingly, despite the
156 different photodegradation conditions employed in the current study (*i.e.*, high vacuum and
157 absence of O_2), the extracted E_a corresponding to PbI_2 degradation under Xe lamp illumination
158 (55.2 mW/cm^2) agrees well with the E_a value reported by Dawood *et al.* (4.7 kcal/mol).[10]

159 Further investigations using XRD and XPS techniques revealed that Pb^0 was the remaining non-
160 volatile products from the photodecomposition of PbI_2. More interestingly, this decomposed Pb^0
161 product showed also a reversible recovery process back to PbI_2 after short-time exposure to I_2
162 gas (Supplementary Section S7-S8).

163 In summary, the chemical and physical processes extracted from all the sets of degradation and
164 recovery experiments on PbI_2 powders and thin-films are summarized by Equation 1 as well as

illustrated in Figure 1c. Under illumination with photon energies higher than 2.34 eV (< 530 nm), photodecomposition takes place but it is a reversible process if Pb^0 is exposed again to I_2(g),

$$PbI_2(s) \overset{h\nu}{\leftrightarrow} Pb^0(s) + I_2(g) \quad (1)$$

Under dark condition at moderate temperatures (~70 ºC) in high vacuum (~10^{-6} Torr), PbI_2 sublimates in the form of molecules or clusters as depicted in Figure 1b or described in Equation 2 below,

$$PbI_2\ (s) \overset{\Delta}{\rightarrow} n\ PbI_2(g) \quad (2)$$

Noteworthy, no traces of released I2 gas were observed during dark and mild temperature conditions.

$MAPbI_3$ and $MAPbBr_3$ degradation under illumination and dark conditions.

In the previous section, PbI_2 photodecomposition and its volatile (I_2) and non-volatile (Pb^0) decomposition products as well as recovery routes were established based on our home-built setup. Identical experimental conditions were applied to $MAPbI_3$ perovskite. In addition, we also studied the photodecomposition of $MAPbBr_3$ for comparison purposes as this material has been reported to show higher stability than $MAPbI_3$.[7, 13, 14] Currently, the origin of this difference remains largely elusive and such relative stability has also found contradictory results.[15]

$MAPbI_3$ was introduced in the vacuum chamber and after pumping down the system (~10^{-6} Torr), a set of Xe lamp illumination light pulses and only heating pulses under dark condition

experiments were carried out. Sample temperature and MS traces recorded are displayed in Figure 2a,b for each experiment. Firstly, it was striking to note that the hybrid perovskites required much longer time (~72 h) to reach a similar level of high vacuum condition compared to PbI_2 (~6 h). MS data helped to clarify the reason of this phenomenon. One of the most important findings from this experiment is that in contrast with PbI_2, $MAPbI_3$ powder sample releases I_2 independently of light or dark conditions. The rate of I_2 generation was relatively constant during the light/dark pulse conditions (Figure 2a), whereas I_2 was only generated at high temperature pulses (> ~60 ^oC) applied during heat-in-dark condition (Figure 2b). Under mild temperature conditions (< ~60 ^oC), I_2 release is minimized. This indicates that $MAPbI_3$ continues to degrade for a while once it is exposed to the light source. Unlike PbI_2, $MAPbI_3$ does not have a threshold in wavelength where I_2 is released by photodecomposition. If this threshold exists because the band gap on $MAPbI_3$, an infrared light source should be used and therefore we prefer to use directly heating the sample in dark conditions. Furthermore, in addition to I_2 release, $MAPbI_3$ perovskite was continuously releasing the organic gas components (CH_3NH_2, HI, CH_3I and NH_3) under vacuum conditions. Upon $MAPbI_3$ insertion into the vacuum chamber, the background signals associated to $MAPbI_3$ degradation detected by MS were observed to increase. Such an increase was further enhanced during the pulse rises of light or temperature. Furthermore, mass peaks corresponding to dimethylformamide (DMF) solvent can be observed.[16] Such occluded solvent molecules in the perovskite were expected to be detected because perovskite powder samples were prepared by using a protocol similar to the typical spin coating deposition method, see Methods and Supplementary Section 1. E_a values for the I_2 release in $MAPbI_3$ were extracted to compare with the PbI_2 case, see Table 2.

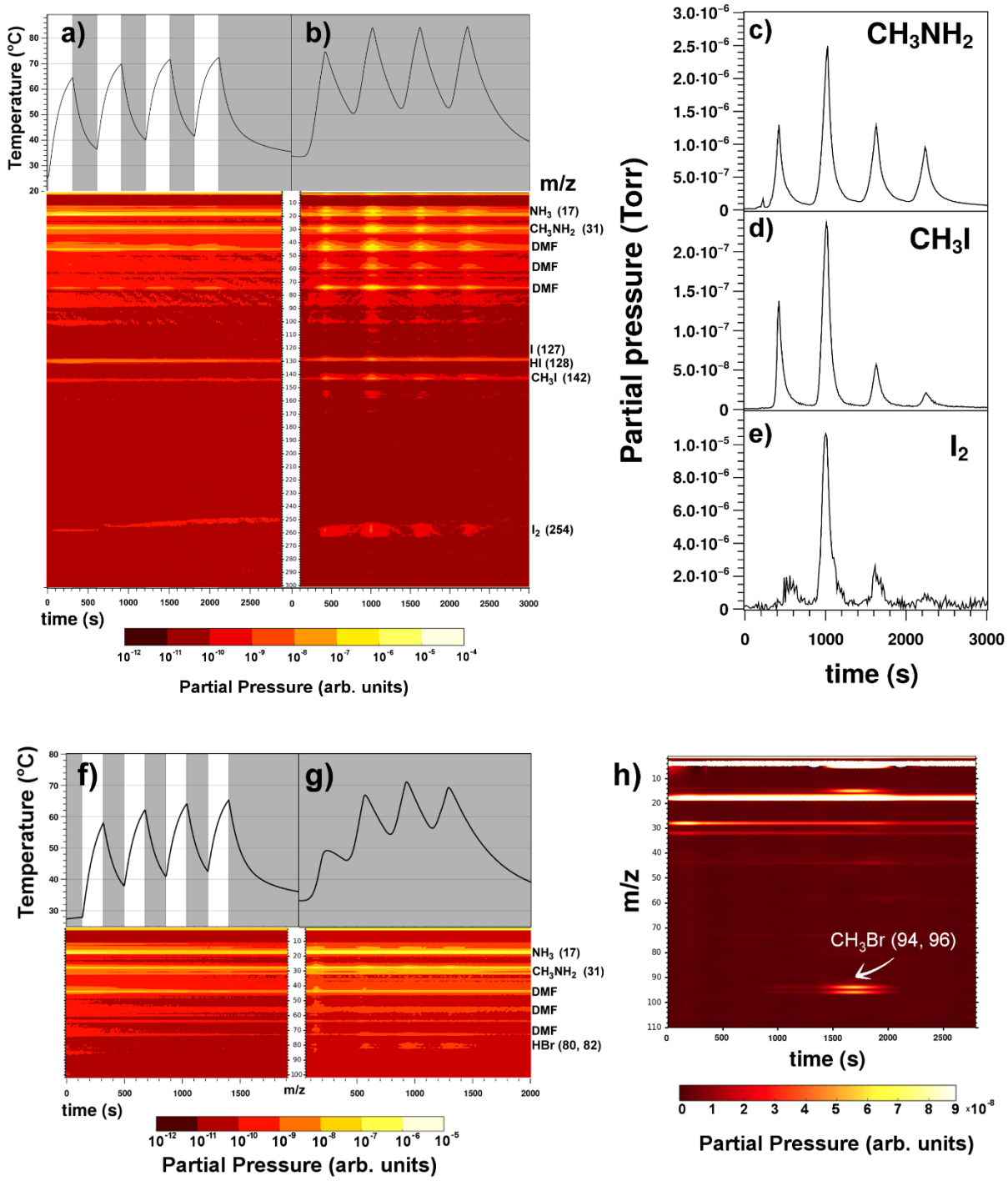

209

210 **Figure 2 | Mass spectrometry profiles of $MAPbI_3$ and $MAPbBr_3$ decomposition products**
211 **during illumination and heating-at-the-dark pulses experiments.** a) Light/dark intervals (5
212 min each) on $MAPbI_3$ perovskite sample using a Xe lamp delivering 55 mW/cm^2 of light power.
213 White and grey areas represent under light and dark pulse duration, respectively. The black lines
214 correspond to the sample temperature. b) Heating on/off intervals (5 min each) on $MAPbI_3$

sample under dark conditions. Species of interest detected in MS are labeled in the right side. Right panel shows calibrated mass traces for c) CH_3NH_2, d) CH_3I and e) I_2 during the heating intervals in dark conditions. Supplementary Figure S14 shows calculated CH_3I/CH_3NH_2 molar ratio. f) Light/dark intervals (3 min each) on $MAPbBr_3$ perovskite sample. g) Heating on/off intervals (3 min each) on $MAPbBr_3$ sample. h) m/z traces registered simultaneously during the thermal degradation of $MAPbBr_3$ using a heating rate of 20 °C·min^{-1} under He atmosphere in a TG/DTA equipment using the same setting as recently published for $MAPbI_3$ perovskite.[9] Release of CH_3Br (m/z = 94 and 96 amu traces) is observed during the thermal degradation. Supplementary Figure S13f shows the fragmentation pattern for CH_3Br molecule.

Table 2. Estimated* activation energies (kcal/mol) for the degradation reactions releasing I_2 in $MAPbI_3$ samples as measured by MS spectrometry.

Light/dark conditions	Temperature (°C)	Light Intensity (mW/cm^2)	E_a (kcal/mol)
Xe lamp	35-72	55	6
Heat in dark	60-84	0	18

*Details on E_a determination and wavelength spectra for each light source are shown in Supplementary Sections S4 and S5, respectively.

Interestingly, the E_a value corresponding to I_2 release in $MAPbI_3$ (~6 kcal/mol) was slightly lower to that in PbI_2 (~9 kcal/mol), which indicates that I_2 release in $MAPbI_3$ is even slightly more favorable than in PbI_2. Because I_2 release was observed in dark conditions, E_a was also calculated for $MAPbI_3$ from I_2 released signal during heating-in-the-dark experiments. We noticed that E_a in the heating in dark condition was around three times higher compared to that of under light exposure meaning that light-driven process is dominant in $MAPbI_3$ degradation phenomena.

Similarities and differences found for $MAPbI_3$ and PbI_2 during these light/heat stress experiments rely on two possible reasons (considering that $MAPbI_3$ material system is at some extent represented by PbI_2 with intercalated MA^+ cations): (i) in contrast to PbI_2, $MAPbI_3$ shows smaller band gap, suggesting that additional photons with lower energies become effective for exciton and/or free charge generation at the same illumination power, and (ii) I_2 release in $MAPbI_3$ does

not need a two exciton mechanism as PbI_2 because [PbI_6] octahedral distortion produces shorter I-I bond distances consistent with the formation of neutral I_2 defects,[17] which potentially facilitates the release of I_2.[18]

For the sake of completeness, the same photo-, thermal decomposition experiments performed on PbI_2 and $MAPbI_3$ were applied to $MAPbBr_3$ to elucidate its decomposition products (*e.g.*, is Br_2 generated? What organic molecules are released from degraded $MAPbBr_3$?) and associate it with the reported disparity in the stability of $MAPbBr_3$ compared to $MAPbI_3$. Comparing the experimental observations on photodecomposition between $MAPbI_3$ and $MAPbBr_3$ perovskites, the main difference was that under vacuum and near room temperature conditions, $MAPbI_3$ showed all a plethora of degradation gas products (*i.e.*, CH_3I and NH_3; CH_3NH_2 and HI; and I_2), but $MAPbBr_3$ only released CH_3NH_2 and HBr (and solvent), Figure 2f,g. We emphasize that CH_3Br, NH_3, and Br_2 gaseous species detection were below the signal-sensitivity threshold of MS under vacuum conditions at low temperature range (30-70 ºC). On the other hand, under near atmospheric inert He pressure conditions and at high temperatures (~300 °C), $MAPbI_3$ and $MAPbBr_3$ underwent similar degradation processes of releasing CH_3I/NH_3 gas products ($MAPbI_3$)[9] and CH_3Br/NH_3 ($MAPbBr_3$) (Figure 2h), respectively. Table 3 summarizes both experimental conditions and detected products from degradation tests carried out in perovskites.

Table 3. Summary of experimentally detected volatile degradation products under different environmental conditions. As comparison previously reported degradation products are also indicated in the table.

Perovskite type	Inert atmosphere: Vacuum T ~ room	Inert atmosphere: ~ 1 atm, Helium T ~300 °C
$MAPbI_3$	1) $CH_3NH_2 + HI$ *,‡ 2) $NH_3 + CH_3I$ *,‡,# 3) I_2 *	$NH_3 + CH_3I$ †
$MAPbBr_3$	$CH_3NH_2 + HBr$ *	$NH_3 + CH_3Br$ *

* This work. † Ref. no. 9. ‡ Ref. no. 19. # Ref. no. 20 assuming that an iodine-transfer polymerization reaction was involved on the CH_3I monomer to form radical species as $CH_3CH_2^{\bullet}$ which can propagate to form a longer polyethylene chain as observed in the work by Ke et al.

In summary, the chemical processes extracted from all the sets of degradation and recovery experiments on halide perovskite powders and thin-films are summarized by Equation 3 and 4 as well as illustrated in Figure 1d for $MAPbI_3$. Under illumination or dark low heating conditions compatible with photovoltaic operation, photo-, thermal-decomposition reactions take place as,

$$MAPbI_3(s) \overset{hv\ or\ \Delta}{\longleftrightarrow} PbI_2(s) + Pb^0(s) + I_2(g) + CH_3NH_2(g) + CH_3I(g) + HI(g) + NH_3(g) \quad (3)$$

$$MAPbBr_3(s) \overset{hv\ or\ \Delta}{\longleftrightarrow} PbBr_2(s) + CH_3NH_2(g) + HBr(g) \quad (4)$$

The CH_3X/NH_3 (X = I or Br) molecules are reported to be the thermodynamically driven product of degradation of methylammonium cation,[19] and such degradation is irreversible to form back again MA^+.[9] In contrast, released CH_3NH_2 + HX is considered to be reversible because of its high reactivity in neutralizing back to MA^+ and X^-. In fact, CH_3NH_2/HI gases have been demonstrated as excellent reagents used directly to synthesize $MAPbI_3$ perovskite.[21, 22] Therefore, under encapsulated conditions, the consideration of CH_3NH_2 + HI released gases as

degradation products from perovskites would not be a correct term as they are able to resynthesize $MAPbI_3$. A unique situation where CH_3NH_2 + HX could be considered as degradation products is when perovskites are placed in an open system (*e.g.* non-encapsulated solar cells) where back reaction is obviously inhibited because the released gases are permanently leaked. As highlight from our work, we determined CH_3NH_2 + HI release as a *benign* or reversible pathway of degradation in such a way that it does not lead to the permanent degradation, but to a chemical equilibrium of formation and destruction of perovskite (Figure 1e).

On the other hand, the back formation to MAX or $MAPbX_3$ from the released CH_3X + NH_3 molecules is thermodynamically unfavorable and prone to form non-primary ammonium salts as previously reported.[9] Therefore, we assign the CH_3X + NH_3 release to be an authentic detrimental pathway for perovskite degradation. If such a degradation path is taking place even in smaller proportions as represented in Figure 2c,d or elsewhere,[19] it would be the culprit of short time stability of methylammonium based hybrid perovskites solar cells regardless of employing a careful encapsulation. In view of above points, it can be understood that $MAPbBr_3$ is more stable than $MAPbI_3$ because this detrimental path releasing CH_3Br + NH_3 was not observed when kept at low temperatures, *i.e.*, 40-80 ^oC (see Table 3 and equation no. 4). Consequently, an encapsulated sample of methylammonium based bromide perovskite would be more stable than I-based perovskite under near ambient conditions.

Photo-, thermal instability of pristine perovskite: implications for their operational stability on solar cell devices.

Perovskite thin-films employed in photovoltaic devices under working conditions could follow a different degradation path compared to that of pristine polycrystalline powder samples used in this study. In fact, this study on photo-, thermal-decomposition of perovskites, the light harvester

material is placed on purpose at the at the optimistic and favorable conditions for perovskite stability avoiding contacts with any other compound (e.g., HTL, ETL, dopants used in HTL, moisture or oxygen) and also without any applied bias. At this point it is important to remind that chemical synthesis procedure of pristine perovskite as well as temperature and illumination conditions during the tests can be considered similar to perovskite submitted under working conditions in devices.

In regard to selective contacts, what side reactions are going to suffer for example a specific HTL used in photovoltaic devices upon exposure to these gas by-products (HI, CH_3I, I_2, CH_3NH_2 and NH_3) released for example by $MAPbI_3$ during working conditions (eq. no 3), it is out of scope of this work. However, it is suggested that rarely the spiro functional group in the spiro-MeOTAD molecule, which is widely used as HTL, could resist the attack of these above chemical gas agents during ~20 years of photovoltaic device lifetime. Therefore, avoiding contact with other compounds related only to the device allows to unveil the intrinsic pathways of photo-, thermal-decomposition in perovskite. It could be reasonably considered that the selective contacts could not avoid these intrinsic decomposition paths in perovskites driven by light and temperature. Contrarily, the decomposition would become worst following unknown side reactions specific for each selective layer case.

On the other hand, voltage applied in thin-film is a relevant parameter to take in account when measuring photo-, thermal-degradation in halide perovskites. In regard to degradation paths for perovskite under applied bias, additional experimental work is carried out in a specially designed $MAPbI_3$ thin-film device consisting of two-gold electrode contacts (spaced by 70 microns) deposited on $MAPbI_3$. Controlled bias voltage is applied on the gold electrodes generating an electric field corresponding to that of typically being generated in perovskite solar cells (~0.71

328 V/μm). In this case, perovskite layer is protected from moisture and oxygen by a top CYTOP
329 layer. The core levels of $MAPbI_3$ thin-films were investigated using XPS mapping on lateral
330 devices (Figure 3). As can be seen in Figure 3a, a uniform distribution of Pb^{2+} and I^- belonging
331 to $MAPbI_3$ was found. However, after applying the electric field (Figure 3b) a clear decrease as
332 well as non-uniform distribution in the Pb^{2+} and I^- was observed. XPS spectra (Figure 3c) was
333 also collected from the area between the electrodes (using a 27μm detector slit). A clear
334 formation of Pb^0 and Pb^{2+} depletion was observed in the negative electrode side where reduction
335 process takes place in the perovskite after the externally applied electric field. Similarly, a
336 broadening of the FWHM belonging to I3d core level (from 1.0 to 1.4 eV) was observed after
337 applying the electric field. The broadening of the I3d FWHM indicates formation of new iodine
338 species, such as CH_3I, HI and I_2. Overall, the XPS results in this experiment are consistent with
339 the observations described in the unbiased pristine perovskites case. However, the most
340 impressive fact in these biased thin-film perovskite experiments is the *in situ* observation of
341 violent release of gases observed in the form of "bubbles" formed under the CYTOP transparent
342 layer. The CYTOP layer is effectively impeding such release of volatile gases from perovskite
343 to the ambient. (Figure 3d and deposited video film as SI file).
344

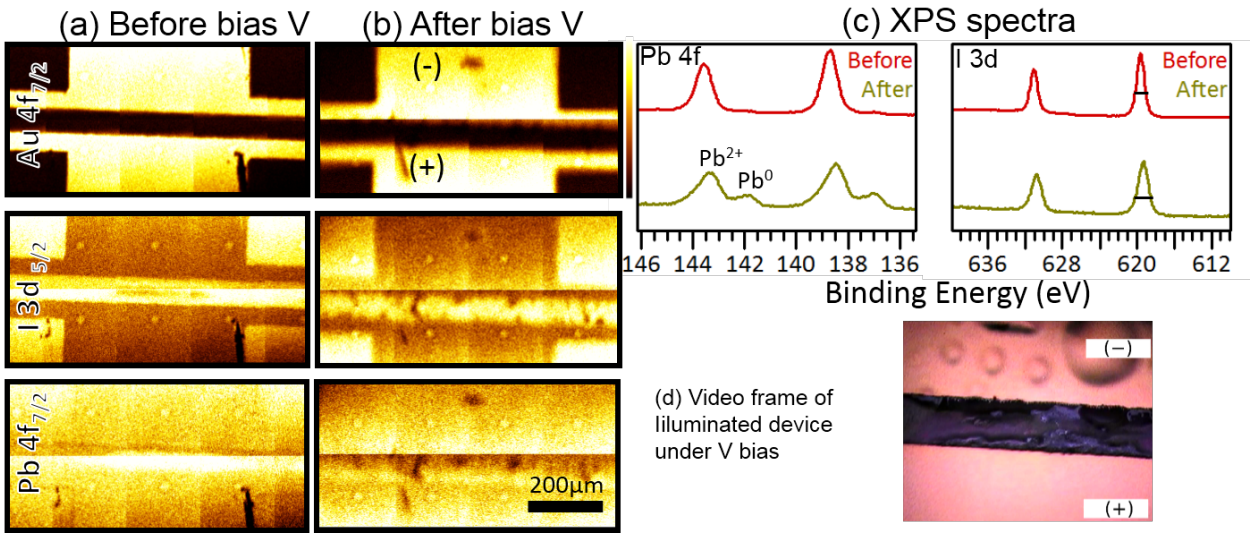

Figure 3. **XPS mapping and spectra (Al-K_α = 1486.6 eV) of $MAPbI_3$ thin films before and after voltage bias.** a, b) XPS maps of Au $4f_{7/2}$, I $3d_{5/2}$, and Pb $4f_{7/2}$ core levels and c) XPS spectra of Pb 4f and I 3d core levels before and after electrical bias. The FWHM of the I 3d peak is 1 eV and 1.4 eV before and after bias applied, respectively. The bias voltage applied is 50 V across 70 µm, ε = 50/70 = 0.71V/µm. Under conventional cell operation at maximum power point, it would be 0.8 V across 0.5 µm of perovskite, ε = 0.8/0.5 = 1.6 V/µm. The Pb^0/Pb^{2+} composition ratio is 0.20 in biased degradation sample. It is similar to 0.18 composition ratio obtained from unbiased sample (see Table S2 and Figure S15b). The composition ratio for I 3d in biased degraded sample is 1.8. This ratio is 1.6 for the unbiased degraded sample (see Table S2 and Figure S17a). d) Video frame of illuminated device under V bias showing the release of volatile gases in the negative electrode and trapped gas bubbles under the transparent CYTOP layer. See SI file for full video of the experiment.

The challenges associated with these chemical instability issues found in $MAPbI_3$ perovskite must be mitigated in perovskite solar cells. Below, four guideline/recommendations based on the outputs of above degradation study could help to design better devices with increased operational stability:

(1) Careful selection of cations for the A site in perovskite structure replacing MA^+ with the proper mixture of Cs^+/FA^+ (cesium and formamidinium) cations. Irreversible reaction

(CH_3I/NH_3 formation and release route) suffered by MA^+ can be solved in principle by replacing it using a mixture of Cs^+/FA^+ (cesium and formamidinium cations) in the A site of perovskite without large efficiency losses. More difficult if not impossible at the moment could be to find an atomic or molecular replacement for the iodide ion still maintaining excellent light harvesting properties.

(2) Encapsulation of devices is necessary not only to avoid contact with external agents, but also to prevent the volatile decomposition products leakage (I_2 for all iodine based perovskites and $CH_3I/NH_3/CH_3NH_2/HI$ for the specific MA^+ based perovskite case). Encapsulation provides that perovskite is inside a thermodynamic closed system allowing only energy exchange and Law of Mass Action stating chemical equilibrium concentrations of solid and gas products according to perceived temperature.

(3) Selective contacts in solar cell, especially organic molecular or polymeric based HTM, must be chosen as chemically inert as possible to be not affected by an environment rich in one of the most acidic molecules (HI), good methylation reagent (CH_3I), oxidizing agent (I_2) and mild to high base as CH_3NH_2 and weak base as NH_3.

(4) In relation to point no. 2 above, hybrid halide perovskite material is assumed to undergo cycles of dynamic formation and decomposition process and this could gradually decrease its crystalline grain size in time. Therefore, efforts on depositing large crystalline perovskite domains could be efforts in vain in regards to the long term stability.

Conclusions

In summary, hybrid lead iodide perovskite has been demonstrated as a semiconductor material that exhibits dynamic processes of continuous decomposition and formation under visible light and/or mild temperature stimulus compatible with solar cells operation conditions. I_2 gas is released from $MAPbI_3$ even in dark conditions during mild heating as low as 40-80 ^oC, which

corresponds to solar cell working temperatures. Fortunately, this photodecomposition reaction is reversible at least for PbI_2, since back formation $Pb^0 + X_2 \rightleftharpoons PbX_2$ is observed. Because $MAPbI_3$ decomposes also into $CH_3I + NH_3$, which corresponds to the irreversible degradation pathway, strategies such as replacement of MA^+ cations by more stable Cs/FA mixed combinations are suggested. $MAPbBr_3$ shows enhanced stability than $MAPbI_3$ because the former decomposes only into $CH_3NH_2 + HBr$ at ambient temperature, which allows a clean self-healing process. Therefore, to further improve the operational stability in hybrid perovskite solar cells, all these photo-, thermal-degradation processes have to be controlled with detailed understanding. Four guideline/recommendations based on the outputs of above degradation study could help to design better devices with increased operational stability. First, the device encapsulation is necessary not only to avoid contact with ambient air, but also to prevent leakage of volatile released products. Second, a careful selection of organic cations in the A site for the compositional perovskite formula is needed to avoid any irreversible reaction. Third, selective contacts must be as chemically inert as possible against volatile released products which could provoke undesired side-reactions. Finally, hybrid halide perovskite material is assumed to undergo a dynamic formation and decomposition process and this could gradually decrease its crystalline grain size with time. Therefore, efforts on depositing highly and large crystalline perovskite could be efforts in vain in regards to the long term stability.

Comment from Authors

During the course of the review of this manuscript (formerly submitted to Nature Chemistry on 14th October 2017), an article (https://doi.org/10.1038/s41563-018-0038-0) appeared describing the enhancement of ion conduction in perovskite by the effect of light. It is a surprising effect

assumed to vacancies generation on perovskite which is better understood based on our MS measurements during soft temperature and light conditions degradation tests.

AUTHOR CONTRIBUTIONS

Y.B.Q. conceived the idea and supervised the work. E.J.J.P. and Y.B.Q. designed the experiments. E.J.J.P. carried out all measurements (except XPS), data analysis, results interpretation, and wrote the first version of the manuscript. L.K.O., M.M. and Z.H performed XPS measurements and assisted with XPS data analysis and interpretation. E.J.J.P. recorded and edited the "bubbling" perovskite video deposited as SI file. All authors assisted with interpretation of the results and contributed to writing the manuscript.

ACKNOWLEDGMENT

This work was supported by funding from the Energy Materials and Surface Sciences Unit of the Okinawa Institute of Science and Technology Graduate University, the OIST Proof of Concept (POC) Program, the OIST R&D Cluster Research Program, and JSPS KAKENHI Grant Number 15K17925. We thank Steven D. Aird, the Technical Editor at Okinawa Institute of Science and Technology Graduate University for valuable suggestions in revising the manuscript.

Methods

Materials. Lead (II) iodide (PbI_2, 99.9%) was purchased from Tokyo Chemical Industry Co., Ltd, lead (II) bromide ($PbBr_2$, 99.999%) was purchased from Sigma-Aldrich, methylammonium iodide (MAI) and methylammonium bromide (MABr) were purchased from Dyesol Limited. All chemicals were used as received without any further purification. Hybrid perovskites in powdered polycrystalline material form were obtained mimicking the procedure to deposit perovskite thin films on substrates. Briefly, 1 mL of DMF (Wako Pure Chemical Industries) solution (~1 M) containing desired stoichiometric precursor quantities to synthesize $MAPbI_3$ or $MAPbBr_3$ was poured on a mortar with 10 cm in diameter and kept at 100 °C inside a fume hood. Precursor solution was slowly spread on the mortar surface helped by the pestle. DMF solvent was evaporated within 1-2 minutes, which resulted in a solid crystalline material on the mortar. The crystal was then carefully collected. Perovskite phase purity (*i.e.* absence of PbI_2) and crystalline parameters were checked from powder XRD measurements (Supplementary Figure S1). Powder XRD were recorded in glazing incidence XRD (GIXRD) mode (detector scan, omega=0.5°) using D8 Bruker Discover (Cu-Kα1 radiation) with 2θ degrees varying from 10° to 55° using 0.5 s of acquisition time for every 0.02° 2θ intervals. Quantitative analysis of powder samples were obtained by fitting the entire XRD pattern with MAUD 2.71 software package.[23]

Photodecomposition experiments. (i) Probing of volatile gases. Fresh samples of PbI_2 (~180 mg) were loaded in the sample holder located inside the chamber (Supplementary Figure S2a). Upon reaching high vacuum level (~10^{-8} to 10^{-6} Torr) monitored by a pressure gauge, MS spectrometer was switched on. The temperature of the sample under dark conditions and high vacuum conditions were slightly high (30-35 °C) due to the e-ionization (radiative heating) of MS. Light power pulses of white, red, and blue LEDs were programmed using Autolab

PGSTAT204 potentiostat including the LED driver box accessory (Metrohm AG). Simulated sun-light was generated using a 150 W short-arc Xe lamp from the Portable Solar Simulator (PEC-L01, Peccell Technologies Inc). Light pulses in the solar simulator were computer controlled remotely by a homemade program and actuator. Light power delivered by both solar simulator and LEDs were calibrated using a calibrated silicon photodiode accounting quartz window and distance from light source to sample holder (Supplementary Section S5 for light power calibration details). Volatile degradation traces were recorded using a quadrupole MS equipped with an electron multiplier detector (SRS Stanford Research Systems, RGA300). Conventional Faraday cup detector in MS was not reliable to detect diiodine traces at nearly room temperature. MS raw signals were calibrated using sensitivity factors calculated following the procedure described in Supplementary Section S6. **(ii) Probing of non-volatile products.** The chemical composition determination of non-volatile products (*i.e.* remaining solid material) from the photodecomposition experiments were performed by XRD and XPS (Supplementary Section S7). The surfaces chemical properties of PbI_2, $MAPbI_3$ and $MAPbBr_3$ were characterized by XPS (Kratos AXIS ULTRA HAS, monochromated Al-Kα = 1486.6 eV) in order to observe the effect of light exposure in vacuum. The binding energy (BE) was calibrated by measuring the Fermi edge (E_F = 0 eV) and Au-$4f_{7/2}$ (84.0 eV) on a clean Au surface. Freshly prepared samples were first analyzed by XPS. The BE scale of PbI_2 spectra was calibrated using the adventitious carbon peak (C 1s) at ~285 eV as reference.[24,25] In our samples, residual amounts of adventitious carbon would be unavoidable due to air exposure prior to the XPS measurements. In addition, C 1s signal originating from residual solvents may be also expected. Great care was taken in order to minimize X-ray exposure time when acquiring XPS signal on PbI_2, $MAPbI_3$, and $MAPbBr_3$ samples. X-ray-induced sample damage was monitored by taking five consecutive scans and comparing these spectra. Acquisition time for each scan varied from 20 to 70 s

depending on the core level regions. The five scans were averaged to a single spectrum if no significant change was observed. Peak fittings and standard deviation calculations were performed with CasaXPS 2.3.16. Shirley function was used to simulate the background signal due to inelastic scattering processes.[26] Raw XPS spectra of Pb 4f, I 3d (for PbI_2 and $MAPbI_3$), Br 3d (for $MAPbBr_3$), C 1s, and N 1s (for $MAPbI_3$ and $MAPbBr_3$) were fitted with Gaussian-Lorentzian (G-L) functions to quantitatively determine BE peak positions, full width at half maximum (FWHM), and the relative spectral areas. The intensity ratios between the $4f_{7/2}$ and $4f_{5/2}$ (Pb) and $3d_{5/2}$ and $3d_{3/2}$ (I and Br) doublets due to spin-orbit coupling were 1.33 and 1.50 (± 3% error), respectively. The concentration of the different elements (metallic-Pb, I, Br, C and N) relative to Pb^{2+} was estimated from the fitted areas after normalization with the atomic sensitivity factors (ASF).[27-29]

A full extension in details experimental section is deposited as ESI including further details in the calibration of light sources used in this work and MS calibration.

References

1. A. Kojima, K. Teshima, Y. Shirai and T. Miyasaka, *J. Am. Chem. Soc.*, 2009, **131**, 6050-6051.
2. Y. Yang and J. You, *Nature*, 2017, **544**, 155-156.
3. G. Grancini, C. Roldan-Carmona, I. Zimmermann, E. Mosconi, X. Lee, D. Martineau, S. Narbey, F. Oswald, F. De Angelis, M. Graetzel and others, *Nature*, 2017, **8**, 1.
4. S. G. Hashmi, A. Tiihonen, D. Martineau, M. Ozkan, P. Vivo, K. Kaunisto, V. Ulla, S. M. Zakeeruddin and M. Grätzel, *J. Mater. Chem. A*, 2017, **5**, 4797-4802.
5. T. Matsui, J.-Y. Seo, M. Saliba, S. M. Zakeeruddin and M. Grätzel, *Adv. Mater.*, 2017.
6. W. Nie, J.-C. Blancon, A. J. Neukirch, K. Appavoo, H. Tsai, M. Chhowalla, M. A. Alam, M. Y. Sfeir, C. Katan, J. Even, S. Tretiak, J. J. Crochet, G. Gupta and A. D. Mohite, *Nat. Commun.*, 2016, **7**.
7. S. Wang, Y. Jiang, E. J. Juarez-Perez, L. K. Ono and Y. B. Qi, *Nat. Energy*, 2016, **2**, 16195.
8. R. G. Wilks and M. Bar, *Nat. Energy*, 2017, **2**, 16204.
9. E. J. Juarez-Perez, Z. Hawash, S. R. Raga, L. K. Ono and Y. B. Qi, *Energy Environ. Sci.*, 2016, **9**, 3406-3410.
10. R. I. Dawood, A. J. Forty and M. R. Tubbs, *Proc. Royal Soc. London A*, 1965, **284**, 272-288.
11. J. Schoonman, *Chem. Phys. Lett.*, 2015, **619**, 193-195.
12. K. Okhotnikov, T. Charpentier and S. Cadars, *J. Cheminform.*, 2016, **8**, 17.
13. R. K. Misra, S. Aharon, B. Li, D. Mogilyansky, I. Visoly-Fisher, L. Etgar and E. A. Katz, *J. Phys. Chem. Lett.*, 2015, **6**, 326-330.
14. R. K. Misra, L. Ciammaruchi, S. Aharon, D. Mogilyansky, L. Etgar, I. Visoly-Fisher and E. A. Katz, *ChemSusChem*, 2016.
15. A. F. Akbulatov, S. Y. Luchkin, L. A. Frolova, N. N. Dremova, K. L. Gerasimov, I. S. Zhidkov, D. V. Anokhin, E. Z. Kurmaev, K. J. Stevenson and P. A. Troshin, *J. Phys. Chem. Lett.*, 2017, 1211-1218.
16. A. E. Williams, P. J. Holliman, M. J. Carnie, M. L. Davies, D. A. Worsley and T. M. Watson, *J. Mater. Chem. A*, 2014, **2**, 19338-19346.
17. J. L. Minns, P. Zajdel, D. Chernyshov, W. van Beek and M. A. Green, *Nat. Commun.* , 2017, **8**, 15152.
18. J. Xie, Y. Liu, J. Liu, L. Lei, Q. Gao, J. Li and S. Yang, *J. Power Sources*, 2015, **285**, 349-353.
19. A. Latini, G. Gigli and A. Ciccioli, *Sustain. Energy Fuels*, 2017, **1**, 1351-1357.
20. J. Chun-Ren Ke, A. S. Walton, D. J. Lewis, A. Tedstone, P. O?Brien, A. G. Thomas and W. R. Flavell, *Chem. Commun.*, 2017, **53**, 5231-5234.
21. S. R. Raga, L. K. Ono and Y. B. Qi, *J. Mater. Chem. A*, 2016, **4**, 2494-2500.
22. S. Pang, Y. Zhou, Z. Wang, M. Yang, A. R. Krause, Z. Zhou, K. Zhu, N. P. Padture and G. Cui, *J. Am. Chem. Soc.*, 2016, **138**, 750-753.
23. L. Lutterotti, R. Vasin and H.-R. Wenk, *Powder Diffr.*, 2014, **29**, 76-84.
24. B. Conings, J. Drijkoningen, N. Gauquelin, A. Babayigit, J. D?Haen, L. D?Olieslaeger, A. Ethirajan, J. Verbeeck, J. Manca, E. Mosconi and et al., *Adv. Energy Mater.*, 2015, **5**, 1500477.
25. B. Philippe, B.-W. Park, R. Lindblad, J. Oscarsson, S. Ahmadi, E. M. J. Johansson and H. Rensmo, *Chem. Mater.*, 2015, **27**, 1720-1731.
26. D. A. Shirley, *Physical Review B*, 1972, **5**, 4709.
27. J. Scofield, *Journal of Electron Spectroscopy and Related Phenomena*, 1976, **8**, 129-137.
28. S. Olthof and K. Meerholz, *Scientific Reports*, 2017, **7**.

29. S. Nakayashiki, H. Daisuke, Y. Ogomi and S. Hayase, *Journal of Photonics for Energy*, 2015, **5**, 057410-057410.

Graphical Abstract